Electronic Supplementary Material (ESI) for Journal of Materials Chemistry A.

Ordered Platinum-Bismuth Intermetallic Clusters with Pt-skin for High Efficient Electrochemical Ethanol Oxidation Reaction

Bin-Wei Zhang, [†a] *Wei-Hong Lai,* [†a] *Tian Sheng,*[b] *Xi-Ming Qu,*[c] *Yun-Xiao Wang,* [*a] *Long Ren,*[a] *Lei Zhang,*[a] *Yi Du,*[a] *Shu-Lei Chou,*[a] *Yan-Xia Jiang,*[c] *Shi-Gang Sun,* [*c] *and Shi-Xue Dou* [a]

[a] Institute for Superconducting and Electronic Materials, Australian Institute of Innovative Materials, University of Wollongong, Innovation Campus, Squires Way, North Wollongong, New South Wales 2500, Australia.

[b] College of Chemistry and Materials Science, Anhui Normal University, Wuhu, 241000, P. R. China.

[c] State key laboratory of physical chemistry of solid surfaces, Department of Chemistry, College of Chemistry and Chemical Engineering, Xiamen University, Xiamen 361005, China

Corresponding Author

*E-mail: yunxiao@uow.edu.au (Y.X.W.).

*E-mail: sgsun@xmu.edu.cn (S.G.S.)

Experimental Section

Synthesis of PtBi/SA Pt and PtBi@Pt

Graphene oxide (GO) was synthesized by Hummers' method. For the preparation of single-atom Pt mixed with PtBi catalyst (PtBi/SA Pt)， the H_2PtCl_6 and $Bi(NO_3)_3 \cdot 5H_2O$ precursors, containing 0.68 mL of 0.039 M H_2PtCl_6 ethanol solution and 0.88 mL of 0.01 M $Bi(NO_3)_3 \cdot 5H_2O$ ethanol solution, respectively, were mixed, and 0.02 g of GO was dispersed in the mixture. The mixture, containing GO, Pt and Bi precursors, were ultrasonicated until ethanol was evaporated; then the mixture was heated 12 h in an oven at 80 °C. Then, the precursors were first reduced at 600 °C in 5 vol % H_2 in nitrogen for 12 h, denoted as PtBi/SA Pt. When further reduced at 600 °C in 5 vol % H_2 in nitrogen for another 12 h, novel monatomic Pt layer on ordered PtBi intermetallic clusters (PtBi@Pt) was formed.

Synthesis of PtBi/C-12 and PtBi/C-24

For synthesis of PtBi supported on XC-72, GO is replaced by carbon black XC-72, and the following processes are the same with PtBi/SA Pt, PtBi@Pt. The 12 h and 24 h thermal treatment are named as PtBi/C-12 and PtBi/C-24, respectively.

Material Characterization

The XRD experiments were carried out on a Rigaku Dmax-3C diffractometer using Cu Kα radiation (40 kV, 30 mA, λ = 0.15408 nm). The X-ray photoelectron spectroscopy (XPS) measurements were conducted on using Al Kα radiation and fixed analyzer transmission mode. The morphology of PtBi/SA Pt and PtBi@*Pt* were investigated by field emission scanning electron microscopy (SEM; JEOL JSM-7500FA), transmission

electron microscopy (TEM) and high-angle annular dark field – scanning TEM (HAADF-STEM; JEOL ARM-200F, 200 keV). The sizes of the PtBi/SA Pt and PtBi@*Pt* particles were measured from about 200 nanoparticles. The loadings of Pt and Bi in the PtBi/SA Pt were determined by nergy dispersive X-ray spectroscopy (EDX) to be about 5.43% and 5.63%; and the loading of Pt and Bi for PtBi@*Pt* was 5.70% and 5.85%, respectively.

Electrochemical testing

A glassy carbon electrode (GC) is polished by Al_2O_3 powder with 5, 1, and 0.3 mm, washed with water under the ultrasonic bath. A certain amount of catalyst (PtBi/SA Pt or PtBi@*Pt*) ink is dropped on a GC electrode, and then left it to dry. Nafion® solution is applied to form a thin layer on the surfaces of the catalysts. For comparison, the commercial Pt/C is prepared by the same process. The electrochemical measurements are conducted on a three-electrode electrochemical cell, a Pt foil as counter electrode, and linked to a PAR 263A potentiostat (EG&G). All electrode potentials have been quoted versus the mercury/mercury oxide reference electrode (Hg/HgO). The solution was de-aerated by bubbling high purity N_2 through it for 15 min before measurements; meanwhile during the experiment, a flow of N_2 is over it to form protection gas atmosphere. The electrochemical experiments are conducted at room temperature.

Electrochemical *in-situ* Fourier transform infrared (FTIR) reflection spectroscopy measurements are carried out on a Nexus 870 spectrometer (Nicolet), and the detector is a cooled MCT equipped with a liquid nitrogen. A CaF_2 disk is applied for the IR

window. A thin layer configuration between the IR window with the working electrode by pushing the working electrode against the IR window before *in-situ* FTIR experiments.[1] *In-situ* FTIR spectra are collected via multi-stepped FTIR spectroscopy (MSFTIR) and single potential alteration FTIR processes. The result spectra are transferring to the relative change in reflectivity, counted as below:

$$\frac{\Delta R}{R} = \frac{R(E_S) - R(E_R)}{R(E_R)}$$

Where R(E_R) and R(E_S) are the independent beam spectra gathered at samples potential E_S and reference potential E_R.

Density functional theory (DFT) calculations

DFT are carried out on a Perdew-Burke-Ernzerhof (PBE) generalized gradient approximation (GGA) exchange-correlation functional through a Vienna Ab-initio Simulation Package (VASP) code.[2-5] A projector-augmented-wave (PAW) pseudopotential is applied to describe the core electron interaction. The cut-off energy was set as 400 eV and the *k*-point sampling for Brillouin zone was 4x4x1. Significantly, the vacuum region layers are built more than 12 Å to make sure the slab interaction is eliminated. Since PtBi is in hexagonal P63/mmc phase, the (0001) surface would be the most stable. The PtBi(0001) surface with single Pt atom site as shown in Figure S1(a), was used as a p(2x2) supercell including 16 Pt and 12 Bi atoms. The Pt(0001) surface with two adjacent Pt atoms was modelled by adding one

extra Pt atom on the single Pt atom exposed surface. As shown in Figure S4(b). The bottom two layer Pt atoms and one layer Bi atoms are fixed in the slab; meanwhile the other atoms are relaxed under the optimization process. The transition states lie in a constrained optimization approach, forcing converge criteria under the 0.05 eV/Å in modified VASP.[6-8]

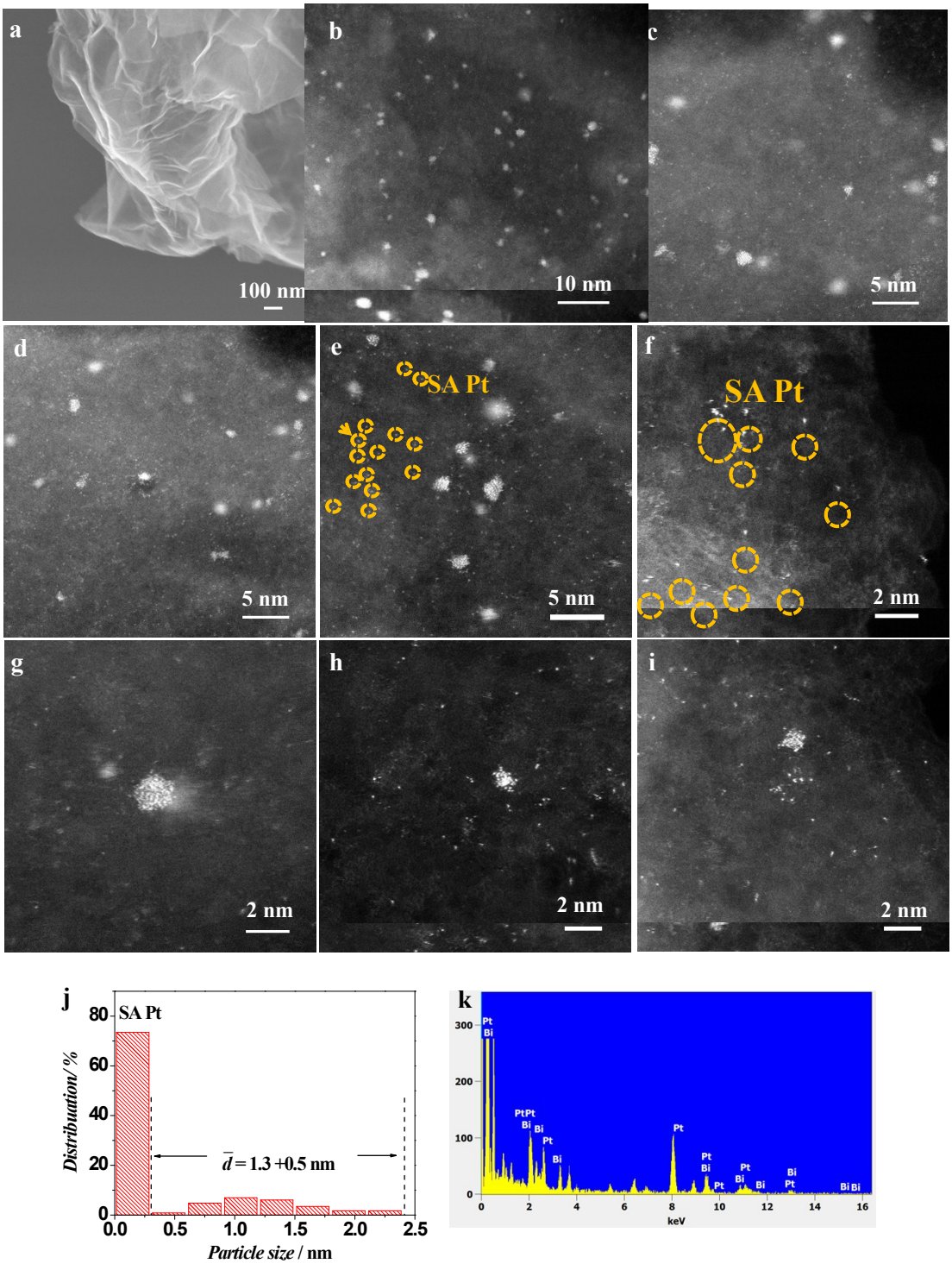

Figure S1. (a) SEM image and (b-i) HAADF-STEM images of PtBi/SA Pt. (j) Histogram of nanoparticle sizes of PtBi/SA Pt. (k) EDS spectrum of PtBi/SA Pt.

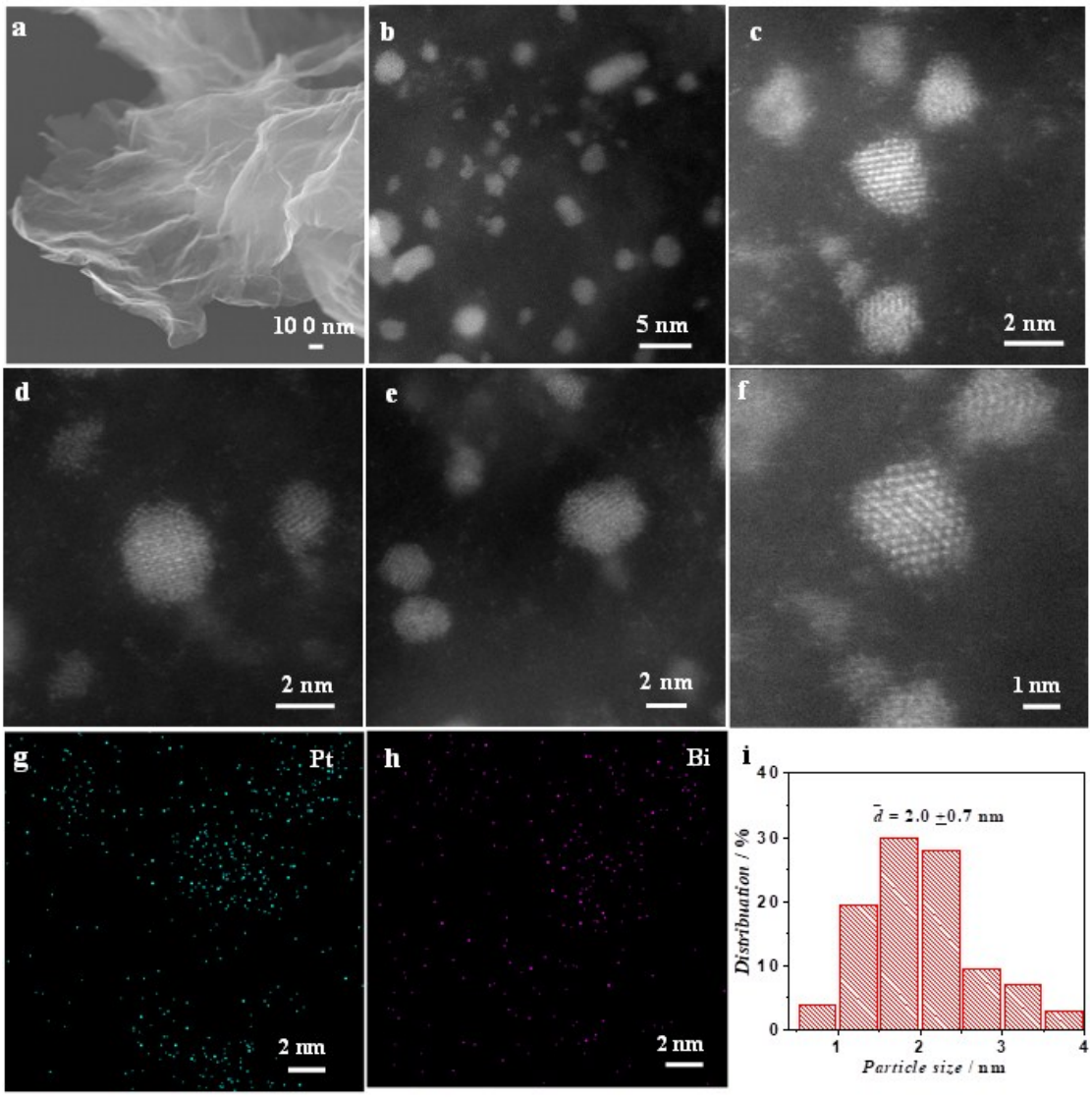

Figure S2. (a) SEM and (b-h) HAADF-STEM images of PtBi@Pt with elemental mapping of Pt and Bi from f; (i) histogram of nanoparticle sizes of PtBi@Pt.

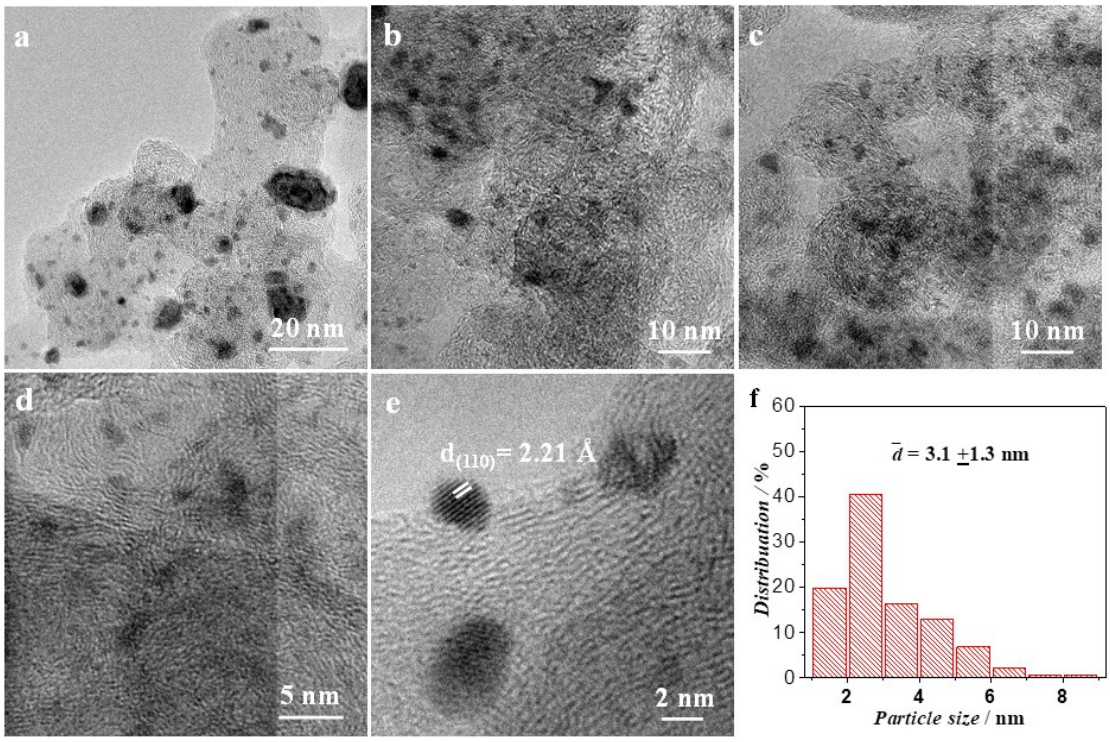

Figure S3. (a)-(b) TEM images of PtBi/C-12; (c) histogram of nanoparticle sizes of PtBi/C-12.

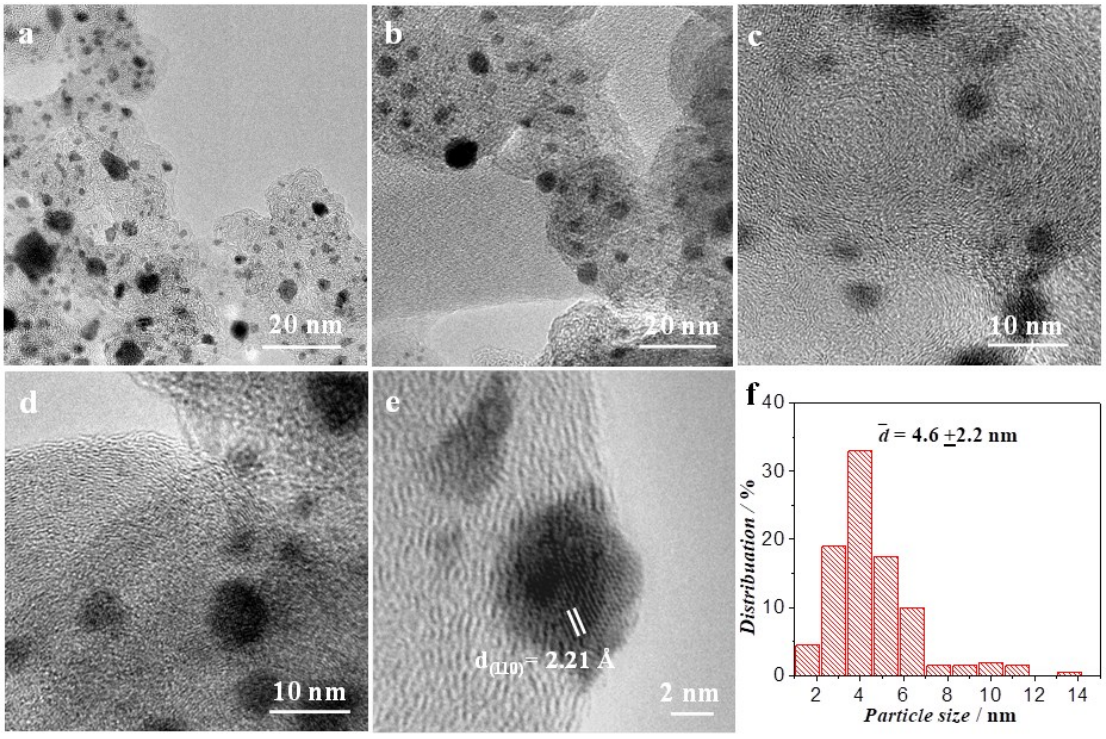

Figure S4. (a)-(b) TEM images of PtBi/C-24; (c) histogram of nanoparticle sizes of PtBi/C-24.

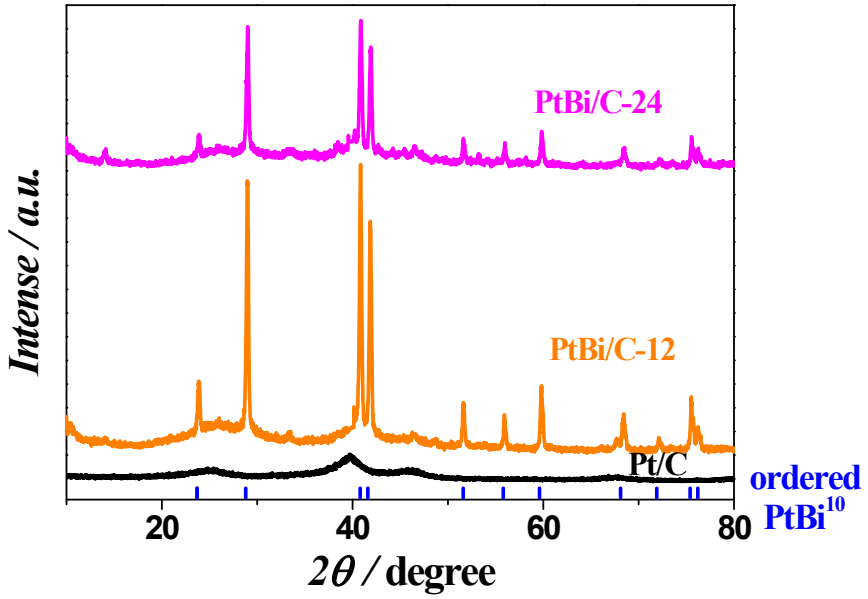

Figure S5. (d) Wide-angle XRD patterns of commercial Pt/C, PtBi/C-12, PtBi/C-24, and ordered PtBi of the reference[3].

To investigate whether the single Pt could be obtained on the carbon black XC-72, which is used as support in commercial Pt/C, we prepared the PtBi/C-12 and PtBi/C-24, as shown in Figure S3 and Figure S4. However, unlike PtBi/SA Pt and PtBi@Pt, it could be clearly seen that both the nanoparticle size of PtBi/C-12 and PtBi/C-24 are inhomogeneous. Nevertheless, most of these two nanomaterials are small nanoparticle; the mean particle size of PtBi/C-12 was determined to be 2.1± 1.3 nm and PtBi/C-24 was 3.3± 2.2 nm. It also indicates that under longer thermal treatment, the nanoparticles will sinter to form large particles.[9] This result is corresponding to the self-assembly phenomena in the PtBi/SA Pt and PtBi@Pt: via 24 h thermal treatment, the SA Pt would self-assemble on the surface of ordered PtBi nanoparticles, formation PtBi@Pt. The XRD of commercial Pt/C, PtBi/C-12, PtBi/C-24, and ordered PtBi of the reference[10] are shown in Figure S5. It demonstrates that the PtBi phase in PtBi/C-12 and PtBi/C-24 are also in ordered PtBi intermetallic phase[10], indicating that this method is an efficient way to prepare order PtBi intermetallic. From HRTEM in Figure S3 and Figure S4, the crystal grains both these two PtBi/C-12 and PtBi/C-24 were clearly observed and the lattice spacing of 0.221 nm was corresponded to the [110] planes of PtBi.[11]

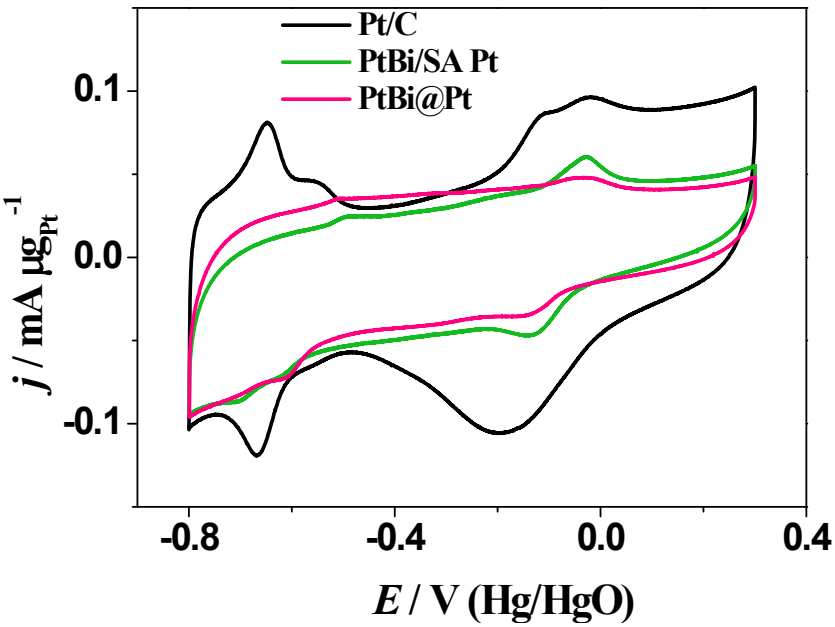

Figure S6. (a) Cyclic voltammograms of catalysts in 1 M KOH, 50 mV s^{-1}: Pt/C (black line), PtBi/SA (green line), and PtBi@Pt (red line).

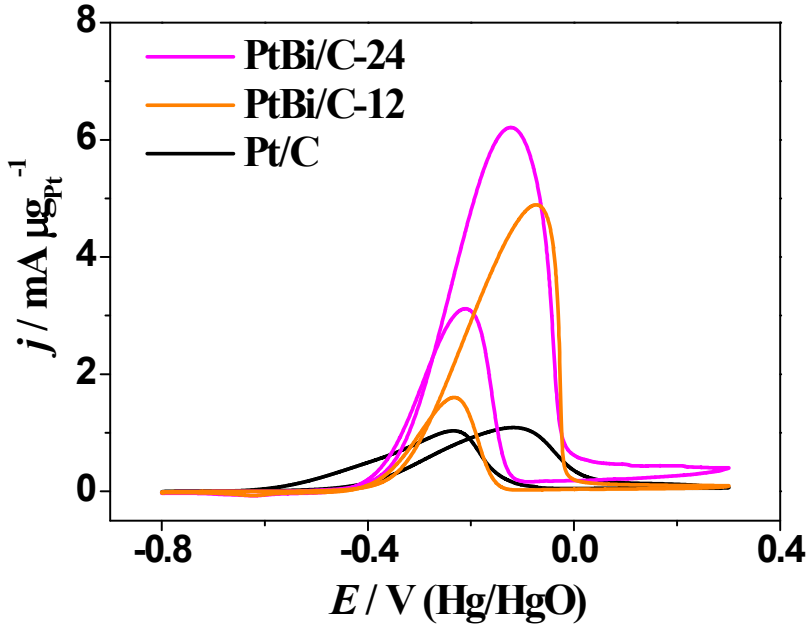

Figure S7. Cyclic voltammograms of catalysts in 1 M KOH + 1 M CH_3CH_2OH, 50 mV s^{-1}: Pt/C, PtBi/C-24, and PtBi/C-12.

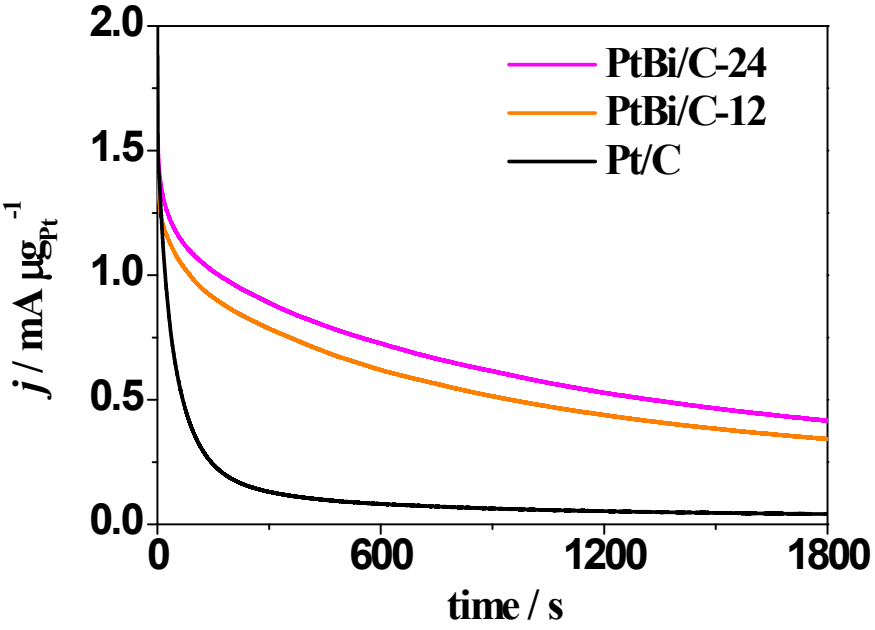

Figure S8. The current-time curves of catalysts in 1 M KOH + 1 M CH_3CH_2OH, 50 mV s^{-1}: Pt/C, PtBi/C-12, and PtBi/C-24.

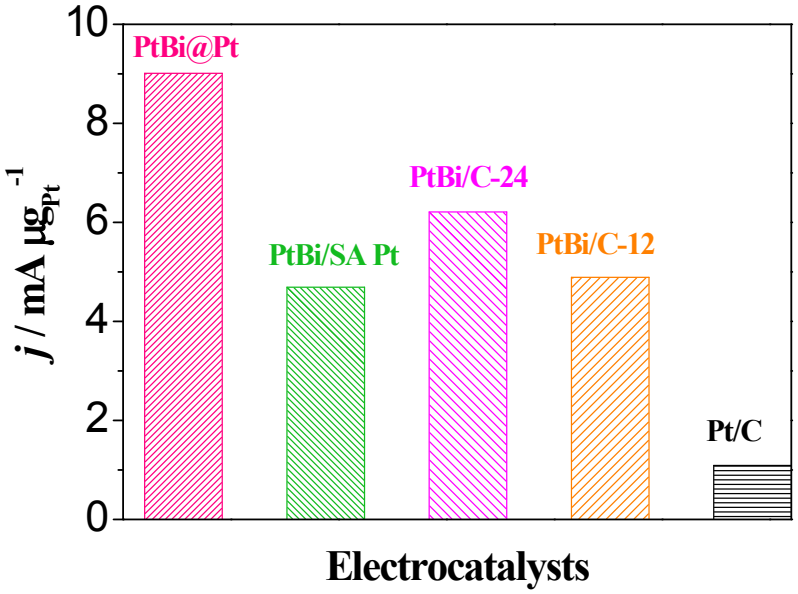

Figure S9. The comparison of mass activities for these electrocatalysts: PtBi@*Pt*, PtBi/SA Pt, PtBi/C-24, PtBi/C-12, and Pt/C at their peak current.

The electrocatalytic characteristics of the EOR for PtBi/C-24 and PtBi/C-12 in 1 M CH_3CH_2OH and 1 M KOH is shown in Figure S7. Significantly, the PtBi/C-24

electrocatalyst shows the higher peak current in the forward anodic scan of 6.21 mA μg_{pt}^{-1} at -0.123 V, when compared with PtBi/C-12 (4.89 mA μg_{pt}^{-1} at -0.074 V), Pt/C (1.09 mA μg_{pt}^{-1} at -0.119). The current-time curves at -0.3 V (Hg/HgO) on PtBi/C-24 and PtBi/C-12 catalysts at room temperature are shown in Figure S8. After 1800 s, the activity of PtBi/C-24 is still higher than those of PtBi/C-12 and Pt/C, demonstrating that PtBi/C-24 possesses better operation stability. The high activity of PtBi/C-24 could be attributed that the surface composition of PtBi/C-24 may via a similar thermal treatment, formation of Pt-rich surface. To get a better understanding of the catalytic activity of these five catalysts for EOR, the current peak of mass activity at 0.90 V was calculated in Figure S9. The mass activity increased in the sequence: Pt/C < PtBi/SA Pt ≈ PtBi/C-12 < PtBi/C-24 < PtBi@Pt. This result also indicates that the PtBi@Pt, with well-sized-distribute, shows better electrochemical performance than that of uneven distributed of PtBi/C-24.

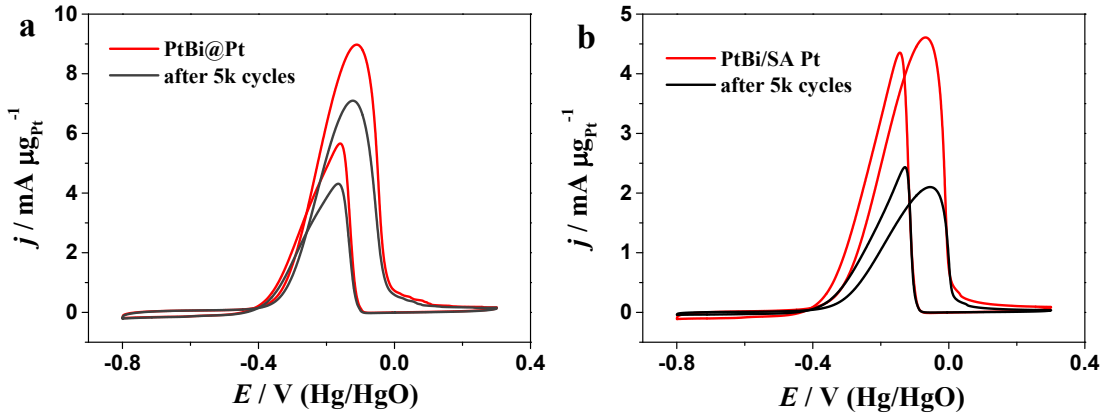

Figure S10. CVs of PtBi@Pt (a) and PtBi/SA Pt (b) before and after 5000 potential cycles between -0.4 and 0.1 V versus Hg/HgO in 1 M KOH + 1 M CH_3CH_2OH solution; scan rate: 50 mV s^{-1}.

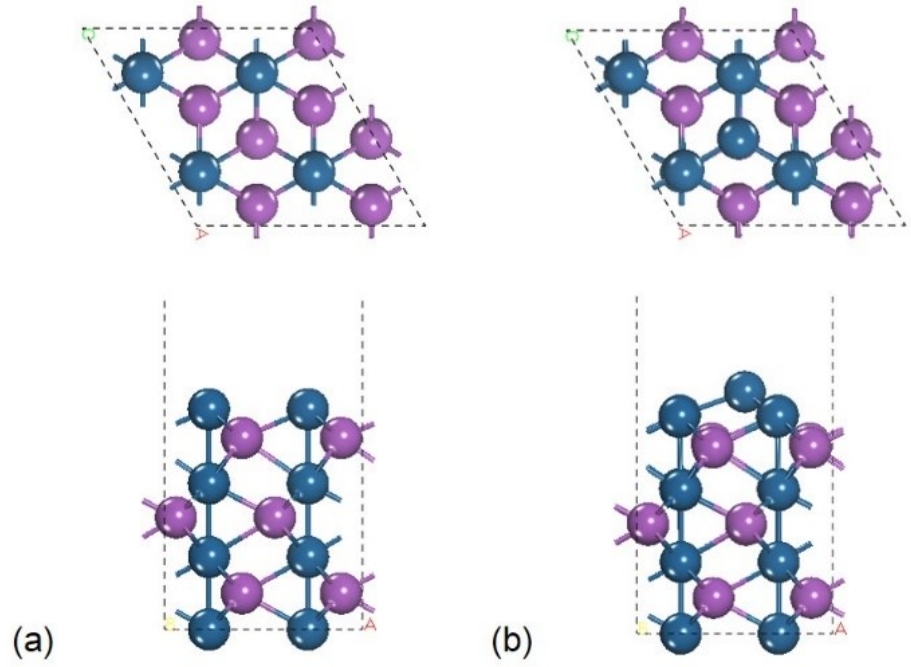

Figure S11. Top and side views of models of PtBi(0001) surface (a) with single Pt atom site, and (b) with two adjacent Pt atoms site. Blue: Pt; purple: Bi.

Table S1. A recent literature survey of the activity of EOR electrocatalysts in alkaline electrolytes.

Electrocatalyst	**Electrolyte**	**Mass activity of Peak current (mA μg_{Pt}^{-1})**	**References**
PtBi@Pt	**1 M KOH + 1 M CH_3CH_2OH**	**9.01**	**This work**
Pd/$Ni(OH)_2$/rGO	1 M KOH + 1 M CH_3CH_2OH	1.546	*Adv. Mater.* **2017**, *29*, 1703057
$Pt_{68}Cu_{32}$ nanoalloy	0.5 M KOH + 0.5 M CH_3CH_2OH	2.33	*Nanoscale*, **2017**, *9*, 2963-2968
Pt black-PbO_2	0.1 M KOH + 0.1 M CH_3CH_2OH	1.162	*New J. Chem.*, **2017**, *41*, 12123
PdCo@NPNCs	1 M KOH + 1 M CH_3CH_2OH	1.245	*J. Mater. Chem. A*, **2017**, *5*, 10876

Au@(Pt + Pd)/C	1 M NaOH + 1 M C_2H_5OH	8.99	*Chem. Commun.*, **2016**, *52*, 374
Pd_2S/C	0.5 M KOH + 0.5 M CH_3CH_2OH	0.162	*J. Power Sources* **2016**, *336*, 1.
Pd_3Sn_1/NG	1 M KOH + 1 M CH_3CH_2OH	3.0	*RSC Adv. 2016, 6, 19314*
$PdCu_2$	0.1 M KOH + 0.1 M CH_3CH_2OH	1.60	*ACS Appl. Mater. Interfaces* **2016**, *8*, 34497.
PdCo NTAs/CFC	1 M KOH + 1 M CH_3CH_2OH	1.49	*Angew. Chem. Int. Ed*. **2015**, *54*, 3669
Pd–PEDOT/GE	1.0 M NaOH + 1.0 M ethanol	4.50	*J. Mater. Chem. A* **2015**, *3*, 1077.
Pd/CB	1.0 M NaOH + 1.0 M ethanol	5.00	*Int. J. Hydrogen Energy* **2015**, *40*, 12382.
Pt-Pd (1:3)/RGO/GC	1 M KOH + 1 M CH_3CH_2OH	1.487	*ACS Appl. Mater. Interfaces* **2014**, *6*, 3607
Pd@CN	1 M KOH + 1 M CH_3CH_2OH	2.52	*Chem. Commun.*, **2014**, *50*, 12637
Pt-Pd CANs	0.5 M KOH + 1 M CH_3CH_2OH	1.08	*J. Mater. Chem. A,* **2014**, *2*, 13840
Pd-Ag nanoparticles	1 M KOH + 1 M CH_3CH_2OH	1.6	*J. Power Sources* **2014**, *263*, 13.
$Pt_{55}Pd_{45}$ bimetallic alloy nanowires	1 M KOH + 1 M CH_3CH_2OH	1.02	*Adv. Mater.* **2012**, 24, 2326
$Bi_{38}@Pt_{63}$/C	0.3 M C_2H_5OH + 0.5 M NaOH	4.8	*Electrochim. Acta* **2017**, 258, 933

$Pt_{50}Bi_{50}/C$	1 M KOH + 1 M CH_3CH_2OH	0.017	*Electrochem. Commun.* **2011, 1**3, 143.
$Pt_{55}Pd_{38}Bi_7/C$	1 M KOH + 1 M CH_3CH_2OH	2.3	*RSC Adv.,* **2016**, 6, 58336.
$Pd_{95}Bi_5/C$	1 M KOH + 1 M CH_3CH_2OH	0.018	*Int. J. Hydrogen. Eenerg.* **2011,** 36, 10522.
$Pd_{20}Bi_1/C$	1 M KOH + 1 M CH_3CH_2OH	5.67	*Electrochim. Acta* **2013**, 99, 22

References:

(1) Rao, L.; Jiang, Y.-X.; Zhang, B.-W.; Cai, Y.-R.; Sun, S.-G. *Phys. Chem. Chem. Phys.* **2014**, 16 (27), 13662.

(2) Kresse, G.; Hafner, J. *Phys. Rev. B,* **1993,** 48, 13115.

(3) Kresse, G.; Hafner, J. *Phys. Rev. B,* **1996,** 54, 13115.

(4) Blochl, P. E. *Phys. Rev. B,* **1994,** 50, 17953.

(5) Kresse, G.; Joubert, D. *Phys. Rev. B,* **1999,** 59, 1758.

(6) Alavi, A.; Hu, P.; Deutsch, T.; Silvestrelli, P. L.; Hutter, J. *Phys. Rev. Lett.,* **1998**, 80, 3650.

(7) Michadelides, A.; Liu, Z. P.; Zhang, C. J.; Alavi, A.; King, D. A.; Hu, P. *J. Am. Chem. Soc.,* **2003**, 125, 370.

(8) Liu, Z. P.; Hu, P. *J. Am. Chem. Soc.* **2003**, 125, 1958.

(9) J. Jones, H. Xiong, A. T. DeLaRiva, E. J. Peterson, H. Pham, S. R. Challa, G. Qi, S. Oh, M. H. Wiebenga, X. I. Pereira Hernández, Y. Wang, A. K. Datye, *Science,* **2016**, *353*, 150.

(10) D. Volpe, E. Casado-Rivera, L. Alden, C. Lind, K. Hagerdon, C. Downie, C. Korzeniewski, F. J. DiSalvo, H. D. Abruña, *J. Electrochem. Soc.* **2004,** *151*, A971.

(11) B.-W. Zhang, C.-L. He, Y.-X. Jiang, M.-H. Chen, Y.-Y. Li, L. Rao, S.-G. Sun, *Electrochemistry Communications* **2012**, *25*, 105-108.